Citation: CPT Pharmacometrics Syst. Pharmacol. (2019) 8, 634–642; doi:10.1002/psp4.12458

ARTICLE

Physiologically-Based Pharmacokinetic Modeling Approach to Predict Rifampin-Mediated Intestinal P-Glycoprotein Induction

Shinji Yamazaki[1,*], Chester Costales[2], Sarah Lazzaro[2], Soraya Eatemadpour[2], Emi Kimoto[2] and Manthena V. Varma[2]

Physiologically-based pharmacokinetic (PBPK) modeling is a powerful tool to quantitatively describe drug disposition profiles *in vivo*, thereby providing an alternative to predict drug–drug interactions (DDIs) that have not been tested clinically. This study aimed to predict effects of rifampin-mediated intestinal P-glycoprotein (Pgp) induction on pharmacokinetics of Pgp substrates via PBPK modeling. First, we selected four Pgp substrates (digoxin, talinolol, quinidine, and dabigatran etexilate) to derive *in vitro* to *in vivo* scaling factors for intestinal Pgp kinetics. Assuming unbound Michaelis-Menten constant (K_m) to be intrinsic, we focused on the scaling factors for maximal efflux rate (J_{max}) to adequately recover clinically observed results. Next, we predicted rifampin-mediated fold increases in intestinal Pgp abundances to reasonably recover clinically observed DDI results. The modeling results suggested that threefold to fourfold increases in intestinal Pgp abundances could sufficiently reproduce the DDI results of these Pgp substrates with rifampin. Hence, the obtained fold increases can potentially be applicable to DDI prediction with other Pgp substrates.

Study Highlights

WHAT IS THE CURRENT KNOWLEDGE ON THE TOPIC?
☑ Physiologically-based pharmacokinetic (PBPK) modeling is increasingly being applied to predict clinical drug–drug interactions (DDIs). Rifampin is a well-known inducer for not only cytochrome P450 (CYP) 3A but also P-glycoprotein (Pgp). PBPK modeling for rifampin-mediated CYP3A induction has been established well whereas that for Pgp induction is still under discussion. Accordingly, a verified PBPK model for Pgp induction is required for rifampin-mediated DDI prediction.

WHAT QUESTION DID THIS STUDY ADDRESS?
☑ The aim of this study was to predict rifampin-mediated fold increases in intestinal Pgp activity via PBPK modeling based on clinically observed DDI results.

WHAT DOES THIS STUDY ADD TO OUR KNOWLEDGE?
☑ PBPK models developed and verified in the present study adequately described clinically observed DDI results of Pgp substrates following multiple-dose administrations of rifampin. The present results will be valuable to understand rifampin-mediated DDI mechanism in the clinic.

HOW MIGHT THIS CHANGE DRUG DISCOVERY, DEVELOPMENT, AND/OR THERAPEUTICS?
☑ The predicted fold induction of intestinal Pgp abundance by rifampin presents advancement toward rifampin-mediated DDI prediction of Pgp substrates in the clinical studies and/or case scenarios that have not yet been tested.

Among the adenosine triphosphate (ATP)-binding cassette-transporters, ABCB1 (P-glycoprotein (Pgp)) is the most extensively studied to date.[1–3] Pgp possesses a broad substrate specificity that substantially overlaps with another ATP-binding cassette-transporter, ABCG2 (breast cancer resistant protein). As Pgp substrates are generally lipophilic, they can, in principle, diffuse passively across biological membranes before the transporters extrude substrates out of cells. Thus, in the absence of active efflux transport systems, Pgp substrates can readily cross membranes and thereafter penetrate into tissues, e.g., pharmacological or toxicological targets. This also means that Pgp-mediated efflux transport activity can only cause significant effects on tissue distribution if efflux transport rates are substantially higher than passive diffusion rates. For some Pgp substrates, Pgp plays a critical role in limiting their oral absorption because Pgp-mediated efflux activity is unlikely saturated due, e.g., to solubility-limited or permeability-limited absorption at clinical doses.[1,2]

Pgp and cytochrome P450 (CYP) CYP3A are expressed in many of the same organs/tissues (e.g., liver and intestine), and there is a substantial overlap in substrate specificity

[1]Pharmacokinetics, Dynamics and Metabolism, Pfizer Worldwide Research & Development, San Diego, California, USA; [2]Pharmacokinetics, Dynamics and Metabolism, Pfizer Worldwide Research & Development, Groton, Connecticut, USA. *Correspondence: Shinji Yamazaki (shinji.yamazaki@pfizer.com)
Received: April 17, 2019; accepted: July 24, 2019. doi:10.1002/psp4.12458

between Pgp and CYP3A, which are both regulated by nuclear receptors such as pregnane X receptor.[1,2,4] It is therefore critical to select the appropriate substrates and interacting drugs on drug–drug interaction (DDI) assessments because the DDI risks should quantitatively be evaluated by accounting for relative contributions of Pgp and CYP3A to overall DDIs.[5,6] Some examples of Pgp probe substrates are digoxin and dabigatran etexilate, which are negligibly metabolized by CYP3A, whereas midazolam is the most commonly used CYP3A probe substrate not transported by Pgp.[7,8] Regarding interacting drugs, it is noteworthy that many dual inhibitors do not have comparable inhibitory potency toward Pgp and CYP3A *in vitro*. For example, amiodarone and felodipine are potent Pgp inhibitors but weak CYP3A inhibitors, whereas itraconazole and ketoconazole are potent inhibitors of both Pgp and CYP3A.[9] On the other hand, multiple-dose administrations of rifampin increase Pgp and CYP3A expression levels by a similar degree, resulting in decreases in systemic exposures of some Pgp and/or CYP3A substrates.[6,10,11] Rifampin-mediated CYP3A induction has been characterized well for DDI prediction.[12,13] In contrast, there has been an increasing need for quantitively predicting rifampin-mediated DDIs with Pgp substrates.

In the present study, we selected four Pgp substrates, digoxin, talinolol, quinidine, and dabigatran etexilate, to investigate the effects of intestinal Pgp-mediated efflux activity on their pharmacokinetics via physiologically-based pharmacokinetic (PBPK) modeling. PBPK modeling is a powerful mechanistic tool to quantitatively describe *in vivo* drug disposition profiles based on drug-dependent and system-dependent parameters.[14,15] Robust PBPK models can extrapolate *in vitro* data to *in vivo* outcomes; therefore, an *in vitro* to *in vivo* extrapolation (IVIVE) of transporter kinetics is key for the successful PBPK modeling of Pgp substrates. Digoxin and talinolol are primarily excreted into urine as unchanged drugs, whereas quinidine is mainly metabolized by CYP3A in liver with moderate renal excretion.[16–18] Dabigatran etexilate is a prodrug and extensively metabolized by ubiquitous carboxylesterases to form the pharmacologically active moiety dabigatran, which is not a Pgp substrate.[19,20] Digoxin and talinolol are categorized into class 3 in biopharmaceutics classification system (BCS) and biopharmaceutics drug disposition classification system (BDDCS), whereas quinidine and dabigatran etexilate are in BCS/BDDCS class 1.[21] Therefore, these substrates are highly soluble in the intestine at clinical doses. We first evaluated the IVIVE factors of the intestinal Pgp kinetic parameters of these substrates via PBPK modeling. According to the general hypothesis that unbound Michaelis-Menten constant (K_m) should be intrinsic, we focused on *in vitro* to *in vivo* Pgp scaling factors (Pgp-SF) for maximal efflux rate (J_{max}) to adequately recover clinically observed pharmacokinetic results. Subsequently, we predicted fold increases in intestinal Pgp abundances (Pgp-FI) by rifampin-mediated induction to adequately reproduce clinical DDI results via PBPK modeling. Our primary objective was to investigate whether Pgp-FIs would be consistent among the selected Pgp substrates. If consistent, we could possibly apply the obtained values to PBPK modeling of other Pgp substrates.

METHODS

Clinical data of Pgp substrates

Intravenous and oral pharmacokinetic results of digoxin, talinolol, quinidine, and dabigatran etexilate including DDI results with rifampin were obtained from the literature. For digoxin, a single dose of digoxin (1 mg) was administered to healthy male participants intravenously over 0.25-hour or 0.5-hour infusion or orally (n = 8–12/group).[22,23] In DDI studies with rifampin, a single oral dose of digoxin (1 mg) was administered to healthy male participants (n = 8/group) after the administration of rifampin (600 mg once daily) for 10 days.[11] For talinolol, a single dose of talinolol was administered to healthy male and female participants (n = 10/group) intravenously (30 mg over 0.5-hour infusion) or orally (100 mg).[24] In DDI studies with rifampin, a single oral dose of talinolol (100 mg) was administered to healthy male participants (n = 8/group) before and after the administration of rifampin (600 mg once daily) for 7–9 days.[25] For quinidine, a single intravenous dose of quinidine lactate (284 mg quinidine over 0.25-hour infusion) was administered to healthy male participants (n = 11/group).[26] In DDI studies, a single oral dose of quinidine sulfate 200 mg (166 mg quinidine) was administered to heathy male participants (n = 6/group) with and without administration of rifampin (600 mg once daily) for 10 days.[17,27] The reported maximal plasma concentration (C_{max}) values in these studies were converted from molar to mass basis, whereas area under the plasma concentration-time curves from time zero to infinity (AUC) values were calculated from the reported clearance values. For dabigatran etexilate, a single intravenous dose of its pharmacologically active moiety dabigatran was administered to healthy male participants (n = 5) over 0.5 hours.[19] In DDI studies, a single oral dose of dabigatran etexilate (150 mg) was administered to healthy male and female participants with and without the administration of rifampin (600 mg once daily) for 7 days (n = 20–24/group).[28,29] In these studies, the pharmacokinetic parameters of total dabigatran (unconjugated and conjugated) were reported, whereas conjugated dabigatran was ~ 20% of total dabigatran based on the assay results before and after alkaline cleavage. The reported values were used in the present study, assuming that the differences were within variability deriving from various factors such as interindividual, intraindividual, and bioanalytical assays based on the meta-analysis.[19,28,29]

In vitro permeability and Pgp kinetics

The apparent *in vitro* passive permeability (P_{app}) of the Pgp substrates digoxin, talinolol, quinidine, and dabigatran etexilate was measured in in-house clonal cells isolated from Madin–Darby canine kidney cells, selected for low endogenous efflux transporter expression (MDCK-LE).[30] Transporter kinetic studies for the Pgp substrates were performed in Caco-2 cells according to the reported method.[6] The Pgp-mediated kinetic parameters K_m and J_{max} were determined by the compartment model analysis, where K_m was defined for unbound concentrations in the cells assuming that the experiments were conducted under sink conditions.[31]

PBPK modeling outline

PBPK modeling approaches in the present study are practically categorized into the following three main tiers: (i) develop PBPK models based on the observed intravenous pharmacokinetic results, (ii) verify the developed PBPK models based on the observed oral pharmacokinetic results, and (iii) apply the verified PBPK models to recover the DDI results with rifampin. The trial designs of the PBPK simulations were primarily set as clinical study designs in the aforementioned reports.

A commercially available dynamic PBPK model, Simcyp population-based simulator (version 17.1; Simcyp Ltd., Sheffield, UK), was used to simulate plasma concentrations of Pgp substrates.[32] The advanced dissolution, absorption, and metabolism model implemented in Simcyp was used to incorporate intestinal Pgp kinetic parameters.[33] The advanced dissolution, absorption, and metabolism model consisting of nine gastrointestinal subcompartments (stomach; duodenum; jejunum I and II; ileum I, II, III, and IV; and colon) integrates physicochemical and biopharmaceutical properties of drugs such as solubility and permeability to predict a fraction of the dose absorbed (F_a) and a fraction of the dose escaping intestinal first-pass metabolism (F_g). Simulation of all clinical trials was performed with a virtual default population of 100 healthy volunteers in 10 trials of 10 participants, each aged 20–50 years with a female/male ratio of 0.5. The output sampling interval in the simulation tool box was set to 0.2 hours in all simulations.

Input parameters of Pgp substrates in the PBPK model

Compound files of talinolol, dabigatran etexilate, and dabigatran were developed and verified based on the aforementioned literature. Default compound files of digoxin, quinidine, and rifampin (multiple-dose rifampicin) from the Simcyp library were used for model verification following some modifications (e.g., Pgp kinetic parameters) as described in the **Supplementary Document**. These compound files were originally developed and verified as a substrate of intestinal and hepatic Pgp for digoxin, a substrate of CYP3A4 as well as an inhibitor of CYP2D6 and CYP3A4 for quinidine, and an inducer of CYP2B6, CYP2C9, CYP2C19, CYP3A4, and CYP3A5 for rifampin. The physicochemical and pharmacokinetic parameters of these substrate drugs are summarized in **Table 1**, whereas those of rifampin are tabulated in **Table S1**.

Sensitivity analysis

In the model development and verification, sensitivity analyses for intestinal Pgp kinetic parameters were performed to adequately recover clinically observed results. Assuming unbound K_m to be intrinsic, *in vitro* to *in vivo* Pgp-SFs for J_{max} were obtained by the sensitivity analyses for ratios of transporter activity or abundance between *in vitro* and *in vivo* (relative activity/expression factor (RAF/REF), in Simcyp). For the DDIs of Pgp substrates with rifampin, sensitivity analyses for Pgp J_{max} were performed to predict rifampin-mediated Pgp-FI assuming that Pgp-mediated efflux activity would increase proportionally with increasing Pgp abundances.

Data analysis

Plasma concentrations of digoxin, talinolol, quinidine, and dabigatran were extracted from the aforementioned reports via DigitizeIt v2.3.3 (Braunschweig, Germany). The C_{max}, time to reach C_{max}, and AUC of Pgp substrates are

Table 1 Physicochemical and pharmacokinetic parameters of digoxin, talinolol, quinidine, dabigatran etexilate, and dabigatran

Parameter (units)	DIG	TAL	QUI	DABE	DAB
Molecular weight	781 (cal)	364 (cal)	324 (cal)	628 (cal)	472 (cal)
LogP	1.26 (ref)	3.15 (cal)	2.81 (ref)	3.8 (ref)	0.063 (cal)
pK_a (base)	Neutral	9.43 (ref)	4.2 & 8.8 (ref)	4.0 & 6.7 (ref)	12.4 (ref)
pK_a (acid)	Neutral	–	–	–	4.4 (ref)
B/P	1.1 (ref)	0.94 (ref)	0.82 (ref)	1.3 (pred)	0.67 (ref)
$f_{u,plasma}$	0.71 (ref)	0.45 (ref)	0.20 (ref)	0.07 (ref)	0.65 (ref)
$P_{eff,man}$ (10^{-4} cm/second)[a]	0.72 (cal)	0.22 (cal)	5.1 (cal)	5.2 (cal)	–
Q_{gut} (L/hour)	5.0 (cal)	1.8 (cal)	15 (cal)	15 (cal)	–
$f_{u,gut}$	1 (def)	1 (def)	1 (def)	1 (def)	–
V_{ss} (L/kg)	6.1 (pred)	2.8 (pred)	2.4 (pred)	17 (pred)	0.63 (pred)
CL_{int}	HHEP/Bile[b]	HHEP/Bile[c]	HLM[d]	CES1/2[e]	HHEP[f]
CL_{renal} (L/hour)	9.7 (ref)	21 (ref)	5.3 (ref)	–	7.2 (ref)
Pgp K_m (μM)	25 (meas)	37 (meas)	1.0 (meas)	2.6 (meas)	–
Pgp J_{max} (pmol/minute/cm^2)	128 (meas)	155 (meas)	21 (meas)	25 (meas)	–

Input parameters are cited from references (ref) indicated in the **Supplementary Document**: digoxin (DIG), S11, S12; talinolol (TAL), S3, S4, S5, S7; quinidine (QUI), S13, S14, S21, S22; dabigatran etexilate (DABE), S8, S9, S10; and dabigatran (DAB), S8, S9. – indicates not applicable.
B/P, blood-to-plasma concentration ratio; cal, calculated; CL_{int}, intrinsic clearance; CL_{renal}, renal clearance; def, Simcyp default; $f_{u,gut}$, unbound fraction of drug in gut; $f_{u,plasma}$, unbound fraction of drug in plasma; J_{max}, maximal efflux rate; K_m, Michaelis-Menten constant; LogP, partition coefficient; meas, measured; $P_{eff,man}$, effective permeability in human jejunum; pK_a, ionization constant; Pgp, P-glycoprotein; pred, predicted or estimated from the clinical results; Q_{gut}, nominal flow in gut model; V_{ss}, steady-state volume of distribution.
[a]Calculated from the measured P_{app} values ($P_{eff,man}$ of 4.1×10^{-4} cm/second in final PBPK models). [b]Additional CL_{int} (0.37 μL/minute/M cells) in human hepatocytes (HHEP) and biliary CL_{int} (0.2 μL/minute/M cells). [c]Additional CL_{int} (0.076 μL/minute/M cells) in HHEP and biliary CL_{int} (1.8 μL/minute/M cells). [d]CL_{int} of 0.24, 0.32, 13, and 1.6 μL/minute/mg protein for cytochrome P450 (CYP) 2C9, CYP2E1, CYP3A4 (3-hydroxylation), and CYP3A4 (N-oxidation), respectively, in human liver microsomes. [e]Recombinant carboxylesterases 1 (K_m = 25 μM, V_{max} = 676 pmol/minute/mg protein) and 2 ($K_{m,u}$ = 5.5 μM & V_{max} = 71 pmol/minute/mg protein). [f]Additional CL_{int} (0.29 μL/minute/M cells) in HHEP.

presented as either arithmetic mean, median or geometric mean with standard deviations (SD), ranges, 90% confidence intervals, or percent coefficients of variation according to the literature. In the DDI studies with rifampin, the ratios of C_{max} and AUC in the test groups relative to control groups ($C_{max}R$ and AUCR, respectively) are presented as either arithmetic or geometric mean ratios according to the literature. To evaluate the predictive model performance, the deviation of the predicted from the observed values was calculated as prediction error (PE):

$$PE\% = \frac{\text{Predicted Value} - \text{Observed Value}}{\text{Observed Value}} \times 100$$

A PE of ≤±25% was provisionally used as the predefined criteria for the model verification.[15,34,35]

RESULTS

The model development and verification of digoxin, talinolol, quinidine, and dabigatran etexilate are summarized in the **Supplementary Document**. This includes PBPK modeling results of intravenous and oral pharmacokinetic data using the *in vitro* Pgp kinetic parameters determined in house (**Table S2–S4** and **Figures S1–S3**).

PBPK modeling of digoxin

The PBPK model-predicted plasma concentration-time profiles of digoxin adequately matched the observed results in healthy participants after a single intravenous infusion and oral administration (**Figure S1**). The sensitivity analysis for *in vitro* to *in vivo* Pgp-SFs showed that the predicted oral C_{max} and AUC were within ±25% at Pgp-SFs of 1–3 (**Figure S3**). In the DDI study, the model-predicted C_{max} and AUC in the control group were within ±18% of the observed results using a Pgp-SF of 2 (**Table 2**). The predicted $C_{max}R$ and AUCR in the test group were within ±25% of the observed results when Pgp-FIs were 3–5 (**Figure 1**). At a Pgp-FI of 4, the predicted C_{max} and AUC in the test group were within ±15% of the observed results, resulting in PEs of ≤±8% for $C_{max}R$ and AUCR (**Table 2**). PBPK model-predicted plasma concentration-time profiles reasonably matched the observed results in both the control and test groups (**Figure 2**). The

Table 2 Physiologically-based pharmacokinetic model-predicted and observed pharmacokinetic parameters of digoxin, talinolol, quinidine, and dabigatran in humans following a single oral administration with and without multiple-dose administrations of rifampin

Drug	Dose, mg	Group	Analysis	Pgp-SF	Pgp-FI	C_{max}, ng/mL	t_{max}, hour	AUC, ng·hour/mL	$C_{max}R$	AUCR
Digoxin	1	Control	Obs[a]	–	–	5.4 ± 1.9	0.7 ± 0.2	55 ± 12	–	–
			Pred	2	–	4.4 ± 1.4	0.9 ± 0.2	56 ± 16	–	–
			PE %	–	–	–18	–	3	–	–
		Test	Obs[a]	–	–	2.6 ± 0.7	0.9 ± 0.3	38 ± 12	0.48	0.70
			Pred	2	4	2.2 ± 1.0	1.0 ± 0.3	34 ± 16	0.52	0.65
			PE %	–	–	–15	–	–10	8	–6
Talinolol	100	Control	Obs[b]	–	–	328 ± 126	3.4 ± 1.4	2,910 ± 1,000	–	–
			Pred	4	–	312 ± 110	1.4 ± 0.3	2,776 ± 956	–	–
			PE %	–	–	–5	–	–5	–	–
		Test	Obs[b]	–	–	204 ± 87	4.6 ± 1.7	1,883 ± 650	0.62	0.65
			Pred	4	3	173 ± 84	1.6 ± 0.4	1,657 ± 813	0.58	0.65
			PE %	–	–	–15	–	–12	–6	1
Quinidine	166 mg	Control	Obs[c]	–	–	616 (487–779)	1.0 (0.5–2.1)	6,640 (3,132–7,905)	–	–
			Pred	5	–	724 (676–776)	1.0 (0.7–1.8)	6,194 (5,682–6,754)	–	–
			PE %	–	–	17	–	–7	–	–
		Test	Obs[c]	–	–	195 (97–227)	0.6 (0.5–4.0)	751 (437–907)	0.32	0.11
			Pred	5	4	180 (155–209)	0.7 (0.4–1.3)	759 (643–895)	0.25	0.12
			PE %	–	–	–7	–	1	–21	8
Dabigatran etexilate	150 mg	Control	Obs[d]	–	–	110 (69)	2.0 (1.5–3.0)	899 (60)	–	–
			Pred	55	–	95 (84)	2.6 (1.1–4.6)	1,022 (88)	–	–
			PE %	–	–	–14	–	14	–	–
		Test	Obs[d]	–	–	38 (72)	2.0 (1.5–4.0)	297 (48)	0.35	0.33
			Pred	55	3	33 (87)	2.9 (1.1–4.6)	363 (92)	0.35	0.35
			PE %	–	–	–12	–	22	1	7

– indicates not reported or calculated.
AUC, area under the plasma concentration-time curves from time zero to infinity; AUCR, AUC ratio in test group to control group; C_{max}, maximal plasma concentration; $C_{max}R$, C_{max} ratio in test group to control group; IV, intravenous infusion; PO, oral administration; Obs, observed; Pred, predicted (n = 100, 10 individuals × 10 groups); PE, prediction error; Pgp-SF, *in vitro* to *in vivo* Pgp scaling factor; Pgp-FI, fold-induction in intestinal Pgp abundances; t_{max}, time to reach C_{max}. [a]Control and test groups (mean ± standard deviation, n = 8/group).[10] [b]Control and test groups (mean ± standard deviation, n = 8/group).[24] [c]Control and test groups (median with range or geometric mean with 90% confidence interval, n = 6/group).[26] [d]Control and test groups (geometric mean with percent coefficients of variation, n = 24).[27]

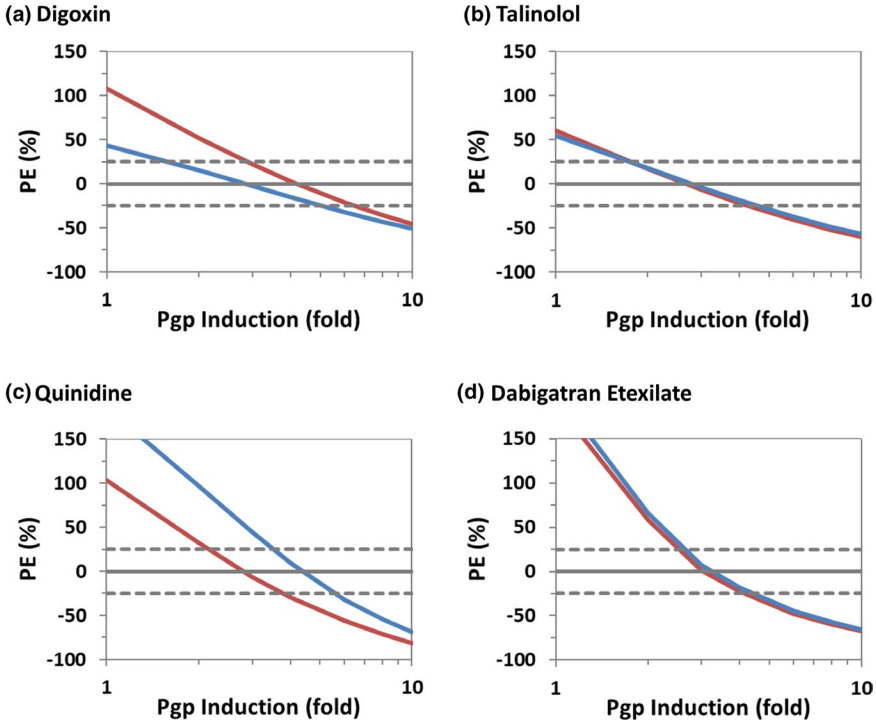

Figure 1 Sensitivity analysis for fold increases in intestinal P-glycoprotein (Pgp) abundances by rifampin-mediated induction on the oral pharmacokinetics of digoxin, talinolol, quinidine, and dabigatran etexilate in healthy volunteers. Single oral doses of digoxin 1 mg (**a**), talinolol 100 mg (**b**), quinidine 166 mg (**c**), and dabigatran etexilate 150 mg (**d**) were administered to healthy subjects with and without multiple-dose coadministrations of rifampin 600 mg once daily. The prediction errors (PE) on the maximal plasma concentration ratios in test groups to control groups (red line) and the area under the plasma concentration-time curve in test groups to control groups (blue line) were calculated by (predicted value – observed value)/(observed value) × 100%. Gray solid and dotted lines represent PEs of 0% and ±25%, respectively.

model-predicted F_a decreased from 0.76 (control group) to 0.45 (test group). Overall, these results suggested that the increase in intestinal Pgp abundances by rifampin-mediated induction would be approximately fourfold in the DDI study of digoxin.

PBPK modeling of talinolol

The PBPK model-predicted plasma concentration-time profiles of talinolol sufficiently matched the observed results in healthy participants after a single intravenous infusion and oral administration (**Figure S1**). The predicted oral C_{max} and AUC were within ±25% at Pgp-SFs of 3–5 (**Figure S3**). In the DDI study, the predicted C_{max} and AUC in the control group were within ±5% of the observed results at a Pgp-SF of 4 (**Table 2**). The predicted C_{max}R and AUCR in the test group were within ±25% of the observed results when Pgp-FIs were 2–4 (**Figure 1**). At a Pgp-FI of 3, the predicted C_{max} and AUC in the test group were within ±15% of the observed results, resulting in PEs of ≤±6% for both C_{max}R and AUCR (**Table 2**). PBPK model-predicted plasma concentration-time profiles reasonably matched the observed results in both the control and test groups (**Figure 2**). The model-predicted F_a decreased from 0.68 (control group) to 0.42 (test group). Accordingly, these modeling results suggested that the rifampin-mediated increases in Pgp abundances would be approximately threefold in the DDI study of talinolol.

PBPK modeling of quinidine

The PBPK model-predicted plasma concentration-time profiles of quinidine adequately matched the observed results in healthy participants following a single intravenous infusion and oral administration (**Figure S1**). The predicted oral C_{max} and AUC were within ±25% at Pgp-SFs of 4–6 (**Figure S3**). In the DDI study, the predicted C_{max} and AUC in the control group were within ±17% of the observed results at a Pgp-SF of 5 (**Table 2**). In the test group, the PEs for C_{max}R and AUCR were within ±25% at Pgp-FIs of 2–4 and 4–6, respectively (**Figure 1**). At a Pgp-FI of 4, the PEs for C_{max} and AUC in the test group were within ±7%, resulting in a PE of –21% for C_{max}R and 8% for AUCR (**Table 2**). The observed mean plasma concentrations were within the 5th to 95th percentiles of the predicted values at a Pgp-FI of 4 (**Figure 2**). The model-predicted F_a, F_g, and fraction of the dose escaping hepatic metabolism and excretion (F_h) were, respectively, 0.63, 0.98, and 0.87 in the control group and 0.25, 0.90, and 0.39 in the test group. Overall, the modeling results suggested that rifampin-mediated increases in Pgp abundances would be approximately fourfold in the DDI study of quinidine.

PBPK modeling of dabigatran etexilate

The PBPK model-predicted plasma concentration-time profiles of dabigatran adequately matched the observed results in healthy participants after a single intravenous infusion of dabigatran (**Figure S1**). The PEs for C_{max} and

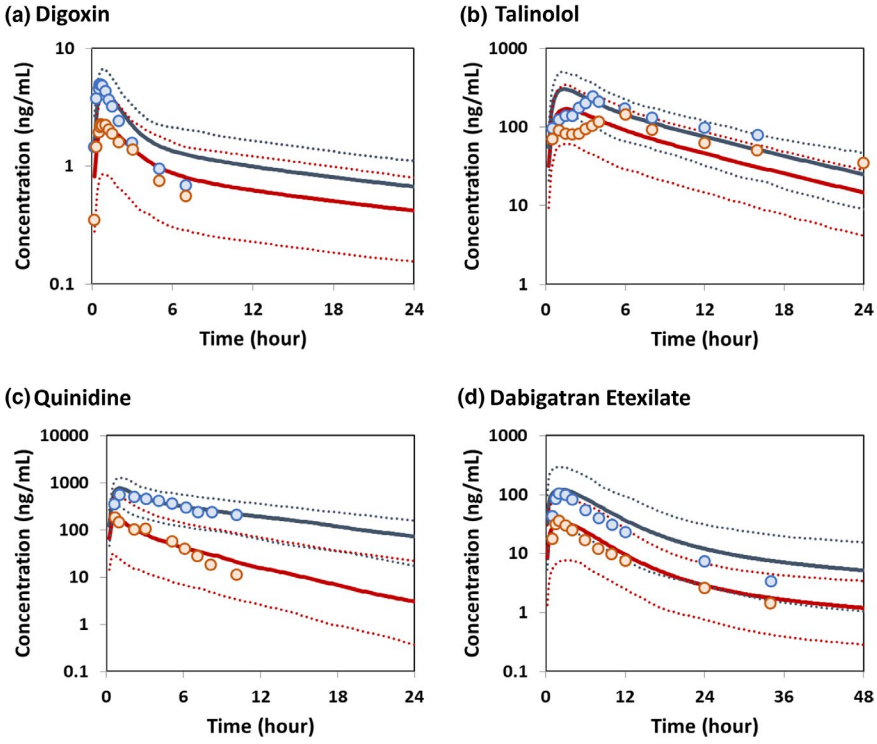

Figure 2 Clinically observed and physiologically-based pharmacokinetic model-predicted plasma concentrations of digoxin, talinolol, quinidine, and dabigatran in healthy subjects following a single oral administration with and without multiple-dose coadministrations of rifampin 600 mg once daily. The oral doses administered were digoxin 1 mg (**a**), talinolol 100 mg (**b**), quinidine 166 mg (**c**), and dabigatran etexilate 150 mg (**d**). The observed and predicted plasma concentrations were expressed as mean (circles) and mean (solid lines) with 5th and 95th percentiles (dotted line), respectively, in the control (blue) and test (red) groups.

AUC were within ±3% (**Table S2**). Following a single oral administration of dabigatran etexilate 150 mg, the predicted C_{max} and AUC were within ±25% at Pgp-SFs of 50–60 (**Figure S3**). In the DDI study, the predicted C_{max} and AUC in the control group were within ±14% of the observed results at a Pgp-SF of 55 (**Table 2**). The predicted C_{max}R and AUCR in the test group were within ±25% of the observed results when Pgp-FIs were 2–4 (**Figure 1**). At a Pgp-FI of 3, the predicted C_{max} and AUC were within ±22% of the observed results, resulting in PEs of ≤±7% for C_{max}R and AUCR (**Table 2**). PBPK model-predicted plasma concentration-time profiles reasonably matched the observed results in both the control and test groups (**Figure 2**). The model-predicted F_a decreased from 0.12 (control group) to 0.04 (test group). Accordingly, the modeling results suggested that rifampin-mediated increases in Pgp abundances would be approximately threefold in the DDI study of dabigatran etexilate as similar to those for other Pgp substrates.

DISCUSSION

We have developed, refined, and verified the PBPK models of four Pgp substrates, digoxin, talinolol, quinidine, and dabigatran etexilate, to derive the rifampin-mediated Pgp-FIs based on the clinically observed DDI results. The proposed modeling approaches appear to be successful in adequately reproducing the observed results. However, the present study clearly underscores the current challenges on PBPK modeling for Pgp substrates. Some potential issues are identified and warrant further investigation and discussion.

One of the most important pharmacokinetic parameters for Pgp substrates is F_a, which is primarily governed by solubility and permeability, including active transport potential. The Pgp substrates tested in this study are categorized into BCS/BDDCS classes 1 or 3, implying that they are highly soluble in the intestine at clinical doses.[21] In the MDCK-LE assay used in this study, a P_{app} value of ≥ 5 $\times 10^{-6}$ cm/second has been proposed as the cutoff for high F_a (≥0.9) in humans.[36] The prediction accuracy was nearly 90% in the results of 97 drugs. The high P_{app} estimates for quinidine and dabigatran etexilate (> 20 $\times$ 10^{-6} cm/second) suggest that their absorption is not permeability limited (**Figure S2**). In contrast, the P_{app} estimates for digoxin and talinolol are below the cutoff (i.e., 3.2 and 0.93 $\times 10^{-6}$ cm/second, respectively). However, the reported correlation analysis between human F_a and P_{app} in the MDCK-LE assay reveals that the observed F_a below the cutoff varies from 0.1–1.[36] Thus, some drugs still exhibit high F_a *in vivo* even though their P_{app} *in vitro* is low. Consistently, the PBPK modeling underpredicted the oral exposures of digoxin and talinolol based on their P_{app} values even though Pgp kinetics were not incorporated into the models (**Tables S3**). The modeling results therefore suggested that *in vivo* intestinal permeability of digoxin and talinolol could be higher than that

predicted from *in vitro* P_{app}. The sensitivity analyses for P_{app} showed steep slopes on the increases in F_a of 0.1–0.9 below the cutoff, i.e., P_{app} of 0.1–5 $\times 10^{-6}$ cm/second corresponding to $P_{eff,man}$ of 0.03–1 $\times 10^{-4}$ cm/second (**Figure S2**). The results clearly represent the marked challenges in quantitatively predicting F_a of low permeable compounds. PBPK modeling with Pgp kinetics can be accomplished with many combinations of $P_{eff,man}$ and J_{max}-SF to recover the observed results unless either was fixed. By taking these findings into consideration, the $P_{eff,man}$ value of Pgp substrates was provisionally set at 4.1×10^{-4} cm/second (P_{app} of ~20 $\times 10^{-6}$ cm/second) in a range of near-complete F_a as summarized in the **Supplementary Document**. Given the challenges on F_a prediction, particularly related to the interplay between passive permeability and transporter-mediated efflux activity, setting a consistent $P_{eff,man}$ value for Pgp substrates could be a practical and experimental approach to model intestinal Pgp effects on absorption in a drug discovery setting when the compounds are prioritized or selected for clinical candidates. However, this approach could potentially underestimate Pgp-SFs for low permeable compounds. Therefore, this approach will (and should) be investigated further with a large set of compounds, particularly including low permeable compounds. Accordingly, the present PBPK modeling approach primarily focused on the effects of Pgp-mediated efflux activity on F_a with minimal impacts of solubility and passive permeability.

The recent reports indicate the current challenges in accurately determining *in vitro* Pgp kinetics largely because of interlaboratory variability derived from various factors such as different cell lines and transporter kinetic equations/models.[37,38] In addition, it has been reported that there was a 2.4-fold difference in Pgp abundances quantified in the same biological samples between two different laboratories.[39] In the present study, the Pgp kinetic parameters were determined by fitting in-house Caco-2 data to the compartmental kinetic models, not by traditional Michaelis–Menten equations.[31,38] The compartmental models can possibly provide consistent Pgp kinetic estimates by accounting for flux through two diffusional barriers with efflux transporters. In the compartment models, K_m is defined for an intracellular unbound concentration and governed by the interaction between substrates and Pgp, providing independent K_m estimates from Pgp expression levels. For instance, the K_m estimates for three Pgp substrates by the compartment models were within twofold in five different monolayer cells, whereas those varied up to nearly 30-fold when estimated by Michaelis–Menten equations with extracellular substrate concentrations.[31] The J_{max} estimates by the compartment models were roughly proportional to Pgp expression levels in these cells. Accordingly, we investigated Pgp-SFs for J_{max} via PBPK modeling to account for the differences in Pgp expression levels or functional activities between *in vitro* and *in vivo* (as IVIVE scaling factors). In contrast, the unbound K_m estimates *in vitro* by the compartment models were assumed to represent *in vivo* affinity, i.e., intrinsic values.

In the PBPK modeling analyses, the estimated Pgp-SFs were relatively consistent (i.e., 2–5) among digoxin, talinolol, and quinidine, whereas it was ~ 55 for dabigatran etexilate. The *in vitro* J_{max} estimates for dabigatran etexilate and quinidine (21–25 pmol/minute/cm^2) were approximately fivefold lower than those of digoxin and talinolol (128–155 pmol/minute/cm^2), whereas the K_m estimates of dabigatran etexilate and quinidine (1.0–2.6 μM) were 10–30-fold lower than those of digoxin and talinolol (25–37 μM) (**Table S1**). Correspondingly, the calculated J_{max}/K_m values among the substrates were within a fivefold range (0.46–2.2 μL/minute/cm^2), implying that dabigatran etexilate Pgp kinetics *in vitro* would not be particularly unique when compared with the other substrates. Clinical doses are also comparable among the substrates (100–166 mg) except for digoxin (1 mg). Thus, the reason for the differences in Pgp-SFs between dabigatran etexilate and other substrates remains unclear. In the clinic, systemic exposures of dabigatran increased proportionally with increasing oral doses of dabigatran etexilate 10–1,200 mg, suggesting only a partial saturation of intestinal Pgp-mediated efflux activity among these doses.[40,41] In contrast, unbound intracellular concentrations of dabigatran etexilate in enterocytes (1–100 μM) calculated with first-order absorption rate constant (k_a) (1 hour^{-1}), F_a (1), unbound fraction of drug in enterocytes ($f_{u,gut}$) (1), and enterocyte blood flow (18 L/hour) were comparable or higher than *in vitro* K_m (2.6 μM), suggesting a possible saturation of Pgp-mediated efflux in enterocytes.[42] The PBPK models assumed that dabigatran etexilate would be converted directly to dabigatran by carboxylesterases 1 and 2. However, dabigatran etexilate, having an ethyl ester and a hexyloxycarbonyl moiety, is rapidly and extensively hydrolyzed to dabigatran via two intermediate metabolites by carboxylesterases.[19,20] Dabigatran etexilate and its intermediates were hardly detectable in human plasma. Taken together, these findings may lead to the hypothesis that carboxylesterase-mediated hydrolysis possibly decreases unbound intracellular concentrations of dabigatran etexilate in enterocytes, resulting in a minimal saturation of intestinal Pgp-mediated efflux activity. Consequently, the PBPK model would likely overpredict Pgp-SFs for dabigatran etexilate by not accurately taking account of carboxylesterase-mediated hydrolysis from the unchanged drug to its metabolites in enterocytes. PBPK models for two intermediates will be pivotal to further understand dabigatran etexilate pharmacokinetics (e.g., F_a and F_g), although there is currently a lack of sufficient data to develop the models.

Rifampin is a well-known modulator for not only drug-metabolizing enzymes but also transporter proteins, including Pgp, leading to complex DDIs with many coadministered drugs.[43–45] Rifampin also has an *in vitro* inhibitory potency for Pgp.[46,47] Multiple-dose administrations of rifampin decreased oral exposures of digoxin by approximately twofold, whereas intravenous exposures were not significantly altered.[11,48] Thus, the decrease in oral exposures would likely be because of rifampin-mediated Pgp induction in the intestine. The present PBPK models reasonably described the DDI results of Pgp substrates with rifampin using Pgp-FIs of 3–4, assuming that Pgp-mediated efflux activity (i.e., J_{max}) proportionally increased with increasing Pgp abundances. Recently, several

rifampin PBPK models have been reported, although Pgp induction was not accounted for in most models.[12,44,49] One of the reported PBPK models sufficiently recovered clinical DDI results of digoxin with rifampin using the similar assumption, i.e., 3.5-fold increase in Pgp J_{max}.[50] Another PBPK model assumed that a maximal increase in rifampin-induced Pgp activity was 2.5-fold.[45] Increases in intestinal Pgp expression levels measured by immunohistochemical and Western blot assays were reported to be 1.4–3.5-fold in healthy volunteers after multiple-dose administrations of rifampin 600 mg once daily.[11] Thus, the predicted rifampin-mediated Pgp-FIs in the present PBPK modeling are roughly consistent with the increases in Pgp abundances in these reports. Overall, the present PBPK modeling results suggest that threefold to fourfold increases in intestinal Pgp abundances could sufficiently reproduce the DDI results of Pgp substrates following multiple-dose administrations of rifampin.

In summary, the present study demonstrated that PBPK models for the Pgp substrates digoxin, talinolol, quinidine, and dabigatran etexilate have reasonably been developed, refined, and verified based on the clinically observed results. The PBPK modeling results suggested that threefold to fourfold increases in intestinal Pgp abundances could sufficiently reproduce the DDI results of Pgp substrates following multiple-dose administrations of rifampin. The derived Pgp-FIs for rifampin-mediated Pgp induction can be valuable to predict or understand rifampin-mediated DDI mechanisms in the clinic. The present results can potentially be applicable to PBPK modeling of other Pgp substrates to predict their pharmacokinetics in the clinical studies and/or case scenarios that have not yet been tested.

Supporting Information. Supplementary information accompanies this paper on the *CPT: Pharmacometrics & Systems Pharmacology* website (www.psp-journal.com).

Supplementary Document
Supplementary Document. Digoxin output, talinolol output, quinidine output, and dabigatran etexilate output.

Acknowledgments. The authors acknowledge Julie Cianfrogna, Theodore Johnson, Rhys Jones, and Ravi Visswanathan (Pharmacokinetics, Dynamics and Metabolism, Pfizer, San Diego, CA) and David Rodrigues (Pharmacokinetics, Dynamics and Metabolism, Pfizer, Groton, CT) for valuable discussions.

Funding. This study was sponsored by Pfizer, Inc.

Conflict of Interest. The authors declared no competing interests for this work.

Author Contributions. C.C., E.K., M.V.V., and S.Y. wrote the manuscript. S.Y. designed the research. C.C., S.E., E.K., S.L., M.V.V., and S.Y. performed the research.

1. Chen, Z. *et al.* Mammalian drug efflux transporters of the ATP binding cassette (ABC) family in multidrug resistance: a review of the past decade. *Cancer Lett.* **370**, 153–164 (2016).
2. Kim, R.B. Drugs as P-glycoprotein substrates, inhibitors, and inducers. *Drug Metab. Rev.* **34**, 47–54 (2002).
3. Agarwal, S., Hartz, A.M., Elmquist, W.F. & Bauer, B. Breast cancer resistance protein and P-glycoprotein in brain cancer: two gatekeepers team up. *Curr. Pharm. Des.* **17**, 2793–2802 (2011).
4. Christians, U., Schmitz, V. & Haschke, M. Functional interactions between P-glycoprotein and CYP3A in drug metabolism. *Expert Opin. Drug Metab. Toxicol.* **1**, 641–654 (2005).
5. Fenner, K.S. *et al.* Drug-drug interactions mediated through P-glycoprotein: clinical relevance and *in vitro-in vivo* correlation using digoxin as a probe drug. *Clin. Pharmacol. Ther.* **85**, 173–181 (2009).
6. Takano, J., Maeda, K., Bolger, M.B. & Sugiyama, Y. The prediction of the relative importance of CYP3A/P-glycoprotein to the nonlinear intestinal absorption of drugs by advanced compartmental absorption and transit model. *Drug Metab. Dispos.* **44**, 1808–1818 (2016).
7. CHMP. Guideline on the investigation of drug interactions <http://www.ema.europa.eu/docs/en_GB/document_library/Scientific_guideline/2012/07/WC500129606.pdf. European Medicines Agency, Committee for Human Medicinal Products (CHMP)> (2012).
8. Center for Drug Evaluation and Research. Clinical drug interaction studies–study design, data analysis, and clinical implications. Guidance for industry (draft) < https://www.fda.gov/downloads/drugs/guidancecomplianceregulatoryinformation/guidances/ucm292362.pdf> (2017).
9. Zhang, L., Zhang, Y. & Huang, S.M. Scientific and regulatory perspectives on metabolizing enzyme-transporter interplay and its role in drug interactions: challenges in predicting drug interactions. *Mol. Pharm.* **6**, 1766–1774 (2009).
10. Yamazaki, S., Loi, C.M., Kimoto, E., Costales, C. & Varma, M.V. Application of physiologically based pharmacokinetic modeling in understanding bosutinib drug-drug interactions: importance of intestinal P-glycoprotein. *Drug Metab. Dispos.* **46**, 1200–1211 (2018).
11. Greiner, B. *et al.* The role of intestinal P-glycoprotein in the interaction of digoxin and rifampin. *J. Clin. Investig.* **104**, 147–153 (1999).
12. Almond, L.M. *et al.* Prediction of drug-drug interactions arising from CYP3A induction using a physiologically based dynamic model. *Drug Metab. Dispos.* **44**, 821–832 (2016).
13. Wagner, C., Pan, Y., Hsu, V., Sinha, V. & Zhao, P. Predicting the effect of CYP3A inducers on the pharmacokinetics of substrate drugs using physiologically based pharmacokinetic (PBPK) modeling: an analysis of PBPK submissions to the US FDA. *Clin. Pharmacokinet.* **55**, 475–483 (2016).
14. Jones, H.M. *et al.* Physiologically based pharmacokinetic modeling in drug discovery and development: a pharmaceutical industry perspective. *Clin. Pharmacol. Ther.* **97**, 247–262 (2015).
15. Shebley, M. *et al.* Physiologically based pharmacokinetic model qualification and reporting procedures for regulatory submissions: a consortium perspective. *Clin. Pharmacol. Ther.* **104**, 88–110 (2018).
16. Wetterich, U. *et al.* Evidence for intestinal secretion as an additional clearance pathway of talinolol enantiomers: concentration- and dose-dependent absorption *in vitro* and *in vivo*. *Pharm. Res.* **13**, 514–522 (1996).
17. Damkier, P., Hansen, L.L. & Brosen, K. Effect of fluvoxamine on the pharmacokinetics of quinidine. *Eur. J. Clin. Pharmacol.* **55**, 451–456 (1999).
18. Iisalo, E. Clinical pharmacokinetics of digoxin. *Clin. Pharmacokinet.* **2**, 1–16 (1977).
19. Blech, S., Ebner, T., Ludwig-Schwellinger, E., Stangier, J. & Roth, W. The metabolism and disposition of the oral direct thrombin inhibitor, dabigatran, in humans. *Drug Metab. Dispos.* **36**, 386–399 (2008).
20. Laizure, S.C., Parker, R.B., Herring, V.L. & Hu, Z.Y. Identification of carboxylesterase-dependent dabigatran etexilate hydrolysis. *Drug Metab. Dispos.* **42**, 201–206 (2014).
21. Benet, L.Z., Broccatelli, F. & Oprea, T.I. BDDCS applied to over 900 drugs. *AAPS J* **13**, 519–547 (2011).
22. Johnson, B.F., Wilson, J., Marwaha, R., Hoch, K. & Johnson, J. The comparative effects of verapamil and a new dihydropyridine calcium channel blocker on digoxin pharmacokinetics. *Clin. Pharmacol. Ther.* **42**, 66–71 (1987).
23. Oosterhuis, B., Jonkman, J.H., Andersson, T., Zuiderwijk, P.B. & Jedema, J.N. Minor effect of multiple dose omeprazole on the pharmacokinetics of digoxin after a single oral dose. *Br. J. Clin. Pharmacol.* **32**, 569–572 (1991).
24. Westphal, K. *et al.* Oral bioavailability of digoxin is enhanced by talinolol: evidence for involvement of intestinal P-glycoprotein. *Clin. Pharmacol. Ther.* **68**, 6–12 (2000).
25. Westphal, K. *et al.* Induction of P-glycoprotein by rifampin increases intestinal secretion of talinolol in human beings: a new type of drug/drug interaction. *Clin. Pharmacol. Ther.* **68**, 345–355 (2000).
26. Greenblatt, D.J. *et al.* Pharmacokinetics of quinidine in humans after intravenous, intramuscular and oral administration. *J. Pharmacol. Exp. Ther.* **202**, 365–378 (1977).
27. Damkier, P., Hansen, L.L. & Brosen, K. Rifampicin treatment greatly increases the apparent oral clearance of quinidine. *Pharmacol. Toxicol.* **85**, 257–262 (1999).
28. Hartter, S. *et al.* Decrease in the oral bioavailability of dabigatran etexilate after co-medication with rifampicin. *Br. J. Clin. Pharmacol.* **74**, 490–500 (2012).

29. Hartter, S., Sennewald, R., Nehmiz, G. & Reilly, P. Oral bioavailability of dabigatran etexilate (Pradaxa((R))) after co-medication with verapamil in healthy subjects. *Br. J. Clin. Pharmacol.* **75**, 1053–1062 (2013).
30. Di, L. *et al.* Development of a new permeability assay using low-efflux MDCKII cells. *J. Pharm. Sci.* **100**, 4974–4985 (2011).
31. Tachibana, T. *et al.* Model analysis of the concentration-dependent permeability of P-gp substrates. *Pharm. Res.* **27**, 442–446 (2010).
32. Jamei, M. *et al.* The Simcyp population-based ADME simulator. *Expert Opin. Drug Metab. Toxicol.* **5**, 211–223 (2009).
33. Jamei, M. *et al.* Population-based mechanistic prediction of oral drug absorption. *AAPS J* **11**, 225–237 (2009).
34. Guest, E.J., Aarons, L., Houston, J.B., Rostami-Hodjegan, A. & Galetin, A. Critique of the two-fold measure of prediction success for ratios: application for the assessment of drug-drug interactions. *Drug Metab. Dispos.* **39**, 170–173 (2011).
35. Yamazaki, S. Relationships of changes in pharmacokinetic parameters of substrate drugs in drug-drug interactions on metabolizing enzymes and transporters. *J. Clin. Pharmacol.* **58**, 1053–1060 (2018).
36. Varma, M.V. *et al.* pH-Dependent solubility and permeability criteria for provisional biopharmaceutics classification (BCS and BDDCS) in early drug discovery. *Mol. Pharm.* **9**, 1199–1212 (2012).
37. Bentz, J. *et al.* Variability in P-glycoprotein inhibitory potency (IC(5)(0)) using various *in vitro* experimental systems: implications for universal digoxin drug-drug interaction risk assessment decision criteria. *Drug Metab. Dispos.* **41**, 1347–1366 (2013).
38. Zamek-Gliszczynski, M.J. *et al.* ITC recommendations for transporter kinetic parameter estimation and translational modeling of transport-mediated PK and DDIs in humans. *Clin. Pharmacol. Ther.* **94**, 64–79 (2013).
39. Harwood, M.D. *et al. In vitro-in vivo* extrapolation scaling factors for intestinal P-glycoprotein and breast cancer resistance protein: part I: a cross-laboratory comparison of transporter-protein abundances and relative expression factors in human intestine and Caco-2 cells. *Drug Metab. Dispos.* **44**, 297–307 (2016).
40. Sanford, M. & Plosker, G.L. Dabigatran etexilate. *Drugs* **68**, 1699–1709 (2008).
41. Eriksson, B.I. *et al.* Dose escalating safety study of a new oral direct thrombin inhibitor, dabigatran etexilate, in patients undergoing total hip replacement: BISTRO I. *J. Thromb. Haemost.* **2**, 1573–1580 (2004).
42. Rostami-Hodjegan, A. & Tucker, G. 'In silico' simulations to assess the 'in vivo' consequences of 'in vitro' metabolic drug–drug interactions. *Drug Discovery Today* **1**, 441–448 (2004).
43. Chen, J. & Raymond, K. Roles of rifampicin in drug-drug interactions: underlying molecular mechanisms involving the nuclear pregnane X receptor. *Ann. Clin. Microbiol. Antimicrob.* **5**, 3–14 (2006).
44. Asaumi, R. *et al.* Comprehensive PBPK model of rifampicin for quantitative prediction of complex drug-drug interactions: CYP3A/2C9 induction and OATP inhibition effects. *CPT Pharmacometrics Syst. Pharmacol.* **7**, 186–196 (2018).
45. Hanke, N. *et al.* PBPK models for CYP3A4 and P-gp DDI prediction: a modeling network of rifampicin, itraconazole, clarithromycin, midazolam, alfentanil, and digoxin. *CPT Pharmacometrics Syst. Pharmacol.* **7**, 647–659 (2018).
46. Prueksaritanont, T. *et al.* Validation of a microdose probe drug cocktail for clinical drug interaction assessments for drug transporters and CYP3A. *Clin. Pharmacol. Ther.* **101**, 519–530 (2017).
47. Reitman, M.L. *et al.* Rifampin's acute inhibitory and chronic inductive drug interactions: experimental and model-based approaches to drug-drug interaction trial design. *Clin. Pharmacol. Ther.* **89**, 234–242 (2011).
48. Gault, H., Longerich, L., Dawe, M. & Fine, A. Digoxin-rifampin interaction. *Clin. Pharmacol. Ther.* **35**, 750–754 (1984).
49. Guo, H. *et al.* A mechanistic physiologically based pharmacokinetic-enzyme turnover model involving both intestine and liver to predict CYP3A induction-mediated drug-drug interactions. *J. Pharm. Sci.* **102**, 2819–2836 (2013).
50. Neuhoff, S. *et al.* Application of permeability-limited physiologically-based pharmacokinetic models: part II - prediction of P-glycoprotein mediated drug-drug interactions with digoxin. *J. Pharm. Sci.* **102**, 3161–3173 (2013).